Proc. of SPIE Vol. 2515, X-Ray and Extreme Ultraviolet Optics, ed. R B Hoover, A B Walker (Jun 1995) Copyright SPIE

Effects of temporal dimensional instability on the Advanced X-ray Astrophysics Facility (AXAF-I) High Resolution Mirror Assembly (HRMA)

Lester M. Cohen

Smithsonian Astrophysical Observatory
60 Garden Street
Cambridge, Massachusetts, USA 02138

ABSTRACT

The NASA Advanced X-ray Astrophysics Facility-Imaging (AXAF-I), one of NASA's Great Observatories, will be launched in 1998. The AXAF-I High Resolution Mirror Assembly (HRMA) will provide sub-arc second imaging resolution over the expected mission life of five years. During assembly and operational life of the telescope, small dimensional changes of the structural support system can degrade the telescopes resolving power by introducing unwanted forces. The forces that are introduced depend, in part, on the long term temporal dimensional stability of the materials that are used in the telescope. A year-long stability study carried out at the University of Arizona Dimensional Stability Laboratory recently concluded. Cyanate ester-based composites, 7050-T7451 aluminum, LR-35 invar, 6Al-4V titanium, 6061-T6 aluminum and Zerodur were studied. The Zerodur material was found to be stable to better than 0.03 PPM/yr. The titanium was found to be stable to better than 0.5 PPM/yr. The 7050-T7451 aluminum and cyanate ester-based composites were found relatively unstable but their instability improved significantly with time. Monte-Carlo (ref 1) and deterministic techniques were used to predict the effects of the instability on the telescopes' performance. Temporal instability effects were within the systems top level requirements.

Keywords: temporal instability, stability, unstrained, room temperature, aluminum, composites, cyanate-esters, invar, titanium, Zerodur

1. INTRODUCTION

The AXAF-I X-ray telescope is composed of a High Resolution Mirror Assembly (HRMA), a Science Instrument Module (SIM), and a 10m long optical bench (OB) metering structure with the HRMA at one end and the SIM at the other end. The HRMA is kinematically mounted to the OB. Therefore, we are concerned with the dimensional instabilities that occur within the HRMA itself and not exterior to the kinematic mount.

The HRMA (fig 1) is composed of four pairs of Wolter Type I grazing incidence X-ray optics supported by an invar and titanium flexure system which in-turn are connected to cyanate-ester based composite mirror support shells (MSS)(fig 2). The invar support pads are adhesively bonded to the outside diameter of each Zerodur mirror. The MSS's are adhesively bonded to an aluminum (7050 T7451) central aperture plate (CAP). Forward and aft of the optics are pre and post collimators (both X-ray and thermal) and supports for X-ray grating experiments. These structures are attached to an aluminum (7050 T7451) outer support cylinder (OSC). The CAP attaches to the OSC and the OSC interfaces to the telescope via three sets of bipod struts.

Dimensional instabilities in aluminum (ref 2) are common, with values in the tens of PPM/yr range for well behaved alloys. Values for invar and titanium are in the range of a less than 1 PPM/yr to a few PPM/yr (refs 3,4). The optic material Zerodur, has been shown to be quite stable; near 0.0 PPM/yr. Non-moisture related data was not available for the cyanate-ester based composite shells, either in the coated or non-coated configuration and therefore its temporal stability was unknown.

Given the symmetric nature of the HRMA, uniform instabilities such as uniform growth in the radial direction of the CAP or MSS, have only minimal effects on the performance of the telescope. Random or non-symmetric deformations can significantly degrade the telescopes' performance because the tangential flexure system can only eliminate radially symmetric errors. We performed sensitivities with unit material instabilities to quantify our concerns. The results indicated that non-uniformities in the CAP and MSS could significantly degrade performance if instabilities of a few PPM/yr over many years were experienced. We were also concerned about the invar mount pads, 12 per optic, which are epoxy bonded to the outside surfaces of the optics . Given the uncertainties with which we were working, NASA/MSFC funded the Smithsonian Astrophysical Observatory (SAO) to conduct this study.

Since the number of samples that were to be tested was large (35) and the degree of accuracy with which the samples had to be measured was high, the University of Arizona (UoA) Dimensional Stability Lab under the direction of Professor S. Jacobs (ref 5) was contracted to perform these measurements. The actual testing at the UoA was performed by T. Peper. The test sample(s) are formed into a Fabry-Perot etalon composed of the sample and end mirrors (ref 6). The optical resonant frequency of this optical cavity is monitored with a dimensionally stable He^{20}-Ne laser. Dimensional changes shift the optical frequency an amount proportional to the strain in the part under measurement. An increase in length lowers the optical frequency.

We used two different geometries as shown in figures 3a & b. The first geometry was a 25mm diameter, 100 mm long solid cylinder with a central hole for the passage of the laser beam. This geometry was used for the 7050 T7451 aluminum, invar and titanium. The second geometry was that of an "open book". The two edges of the book were "tack bonded" together along their "spine" using Tor-Seal adhesive in three small locations. The ends of both types of samples were also polished to provide either a true "optical contact" surface or at least one that would be well seated (between the Fabry-Perot end plates and the samples). The composite samples had their ends coated with SiO prior to polishing. We used the Zerodur samples (see section 3.4) as references to show that the Tor-Seal bonding agent did not cause any unplanned instability. The Zerodur, cyanate-ester composites, and 6061-T6 aluminum were in the "open book" geometry.

2 RESULTS

The performance degradation of the AXAF-I HRMA due to the MSS and CAP temporal instability has been calculated based on the year long test at UofA. An end of life (EOL) X-ray imaging performance degradation of 0.134 arc seconds is predicted , with a top level error budget at EOL of 0.976 arc seconds, 90% diameter, 2-sigma. Resolution is measured by the dispersion of the X-ray photons in the focal plane of the telescope. The AXAF-I top level requirement is to maintain at least 90% of the X-ray photons within a 1 arcsecond diameter, or about 49um, at an X-ray energy of 0.277 KeV.

Tests are currently underway to measure the effects of the invar instability as part of a Zerodur-epoxy-invar system. We have not yet included the effects of the invar pads nor the 7050-T7451 aluminum OSC. We believe that the epoxy may mitigate some of the strain that the invar pads induce into the mirror. The OSC effects will be determined as soon as manpower is available to perform this task.

Eastman Kodak Company (EKC) MSS performance sensitivities documented in HRMA preliminary and critical design reports (ref 7) were used in this analysis and the EKC critical design HRMA performance prediction was used as our baseline. [EKC, a subcontractor to TRW, the prime contractor for AXAF-I, is responsible for the design and development of the telescope assembly, including the HRMA. Hughes Danbury Optical Systems successfully fabricated the flight optics.] SAO performance sensitivities were used for the CAP and are documented in reference 8.

3 DISCUSSION

The test samples were aligned vertically in a vacuum vessel whose temperature was kept at about 27.5C which is just above the nominal use temperature of all of the materials. Temperature variation of the vacuum vessel interior, as measured by the change in length of a copper sample and a platinum resistance thermometer was typically less than +/- 0.010 C. This level of temperature control is quite satisfactory for materials with coefficients of thermal expansion (CTE) of less than about 0.5 PPM/C. However, with high CTE materials, this level of control can introduce measurement errors. The materials with high CTE's (aluminum and titanium) were temperature corrected using the data obtained from the copper reference sample. We assumed that the temperature distribution within the vacuum vessel was the same for all specimens as it was for the copper sample.

Two other reference samples were included with the SAO samples; a fused quartz (SiO_2) sample and an LR-35 invar sample. All three samples (copper, SiO_2, LR-35) have been measured repeatedly over the last 20 years. Both (SiO_2 & LR-35) of these reference samples exhibited excellent long term stability; the SiO_2 sample was < 0.01 PPM/yr and the LR-35 was < 0.10 PPM/yr.

The raw data in terms of frequency vs. time for the 7050 T7451, cyanate-ester composites, invar , titanium, Zerodur, 6061 T6 aluminum and reference materials (SiO_2, LR-35 invar & copper) samples that were tested, are shown in figures 4 through 33. We originally focused only on the composite samples (figs 16 through 19). For these data, the samples are characterized by an increase in frequency (decrease in length) over the first few weeks followed by a slow exponential decay after the initial period. It was believed that the increase in frequency during the initial period was due to loss of moisture but it was subsequently found that many non-composite

samples (fig. 31 for example) also exhibited the same phenomenon . This phenomenon was therefore attributed to a start-up transient which may have been caused by temperature control, vacuum or other issues. Given this start-up transient, the data starting of 23 November, 1993 was used as the starting point for data analysis.

3.1 Central aperture plate 7050 T7451 aluminum

The CAP is nominally 1.32 m diameter by 0.10 m thick including the flanges that attach to the composite MSS. The aluminum samples that were removed from the billet were taken from along one diagonal. At each of three positions, four samples were removed. Two samples were removed from 25mm above the centerline of the plate and two were removed from 25mm below the centerline of the plate. Each pair of two was oriented along the two axes of the rectangular plate (fig 34).

Prior to cryo-aging, the CAP (and stability test samples) were symmetrically rough machined and heat treated at 152C for 8-10 hours. The cryo-aging process consisted of three -84C to +120F cycles. The CAP was cryo-aged three times during its' machining cycle in order to produce as stable a material as possible. The final cycle produced flatness changes of less than 0.02mm. The same cryo-age and machining processes were performed on the cylindrical samples used for stability testing as on the flight CAP.

Figures 35 & 36 shows the converted raw measurements as PPM/yr strains. The top and bottom sample strain rates were also averaged and are shown in figure 37. It was these average values that were used to predict HRMA performance. Figure 38 shows the mean and standard deviation for all of the twelve samples.

In order to determine the effect of these non-uniform strains on the performance of the telescope, we made assumptions as to the distribution of strains in the parts of the aluminum CAP for which we had no data. These assumptions resulted in three different, deterministic distributions. We chose particular distributions based on our understanding of the fabrication processes that were used. Therefore, at each point in time the strain distribution within the CAP was assumed to be one of the three assumed distributions. We consistently found one distribution to be more conservative than the others and used that distribution for performance purposes. Figure 39 shows the results of two of the three distributions and the extrapolation of the predictions out into the future.

The effects of the strains in the CAP are manifested in most cases by deforming the CAP into a potato chip or saddle shape. This then causes the optics to deform in what is termed 'delta-delta-R' which is an ovalization of each end of the optic but with the ends out of phase (nominally 180 degrees).

Numerical analysis of the CAP aluminum material instability data indicated that the functional form of the material instability curve was insensitive to the duration of the instability testing. The exponential equation changed very little whether we used 4 months of test data or 6 months of test data compared with the calculation from 11 months of test data. Figure 40 shows the predicted instability as a function of time when only part of the data was used. Using only the first one third of the data produced an error of about 15% while using only the first one half of the data produced an error of about 7%. Therefore we expect that the derived exponential equations are reasonable and conservative for predicting long term performance as long as the length of time over which we extrapolate is no more than about 5 years. Figure 41 shows the extrapolated instability out to about 3 years. As can be seen, all curves become asymptotic to a zero mean, as one would expect (we do not expect the samples to continue to shrink forever). Table 1 shows the predicted EOL effects for each of the four pairs of optics as well as the entire HRMA.

3.2 Cyanate-ester composites

The Q3 test panel from which these composite samples were taken was fabricated by Hercules Inc. in January '93. Therefore, this panel had "aged" approximately nine months prior to the 23 November, 1993 "start data" date. This test panel was manufactured with a great deal of care and the processes which were used for this panel were carried forward to the flight shells. We use the shell manufacture date and the shell to optic bond date to estimate the individual contribution of each mirror to the expected HRMA performance degradation; the longer the optics will have been bonded to their respective MSS, the greater the degradation. September 1 , 1998 was used as the AXAF-I launch date for performance prediction purposes.

Figures 16 through 19 shows the instability of the composite samples after the effects of moisture have been removed (refs 9,10). Hercules Inc. had postulated (ref 11) that continued moisture loss during the UofA test could be one of the causes for the variability that was seen in the composite data. However, desorbtion of the samples should make the parts shrink, but our parts were growing at a rate

of about 3 PPM/Yr. We postulated, based on discussions with composites experts (refs 12 through 15), that the parts were undergoing stress relaxation due to creep of the 954-3 matrix material. The parts were originally cured at about 163C and have a glass transition temperature (T_G), as measured by the DMA Tan Delta method, of 206C. As the parts cooled down to room temperature, internal residual stresses arose due to the difference in CTE between the matrix and the fibers. The residual stress in the matrix is tensile, since its' CTE is much larger than that of the graphite fibers. A relaxation of this stress, therefore, causes the part to grow. We postulated that if the matrix were fully cured, then the stress relaxation would be quite small. However, the degree of cure of the resin ranges from a low of 78% to a high of 82% for the standard 163C cure cycle (as measured by the infrared and DSC methods) (ref 16) and this may allow the stress relaxation to take place. It is not clear whether post-curing at a higher temperature would reduce the instability since built-in stresses may also increase. However, after a postcure of about 206C, the degree of cure is above 97%.

Each of the exponential fits of the test data, of the form suggested by M. Tuttle (ref 17), were transformed into PPM/yr from MHZ/day by taking the derivative of the F(t) curves and multiplying the instantaneous dF/dt values by -365/474 to arrive at PPM/yr. The 1/474 factor is the UofA provided conversion factor to go from frequency to change in length (MHZ to PPM). Figure 42 shows the derivatives of the original 4 data fits (PPM/yr) extrapolated from the original fabrication date of the Q3 panel (1/93) to several years of mission life. These curves extend out past the EOL of the AXAF-I mission and assume that the form of the exponential equation does not change.

Figure 43 shows the two sigma and minimum to maximum of the four curves as a function of time. The two sigma curves are computed by calculating the standard deviation of the four curves at each time point (i.e. there are four data points for each time) and then multiplying the one sigma result by two. Figure 44 shows the integrated two sigma and zero to peak of the four samples. Figures 45 & 46 show the mean and integrated mean of the four samples. We use two times the one sigma value to determine HRMA performance in keeping with the EKC top level error budget.

The possible errors associated with the small sample size (four) are illustrated in figure 47. In this figure, four probability density functions are shown. The horizontal axis on the figure is the normalized standard deviation. The vertical axis is the probability density. The four curves are for sample sizes of 4, 15, 30 and 100; the samples being drawn from a normally distributed population of random numbers with a mean of zero and a standard deviation of 1.0. With a sample size of only 4, the probability density function is broad and biased below the expected value of 1.0. As the sample size increases, the probability density function becomes more sharply peaked and centered on the expected value of 1.0. By evaluating the integral of the probability density function between 0.0 and 0.50 (since we are predicting on a two sigma basis) for the case of four samples, we are able to estimate the true standard deviation which will exceed the value we obtained using only four samples by about 14%. We, therefore, increased our values by 14% to preclude the possibility of underestimating the performance degradation.

Knowing the time of shell manufacture and shell to optic bonding, the cumulative performance degradation has been estimated based on EKC provided performance sensitivities. Table 2 provides an estimate of the degraded HRMA performance, on a mirror pair by pair basis starting with the XRCF calibration period in November 1996 and extending through the EOL for AXAF-I. The performance degradation is directly related to the length of time between MSS fabrication and MSS to optic bonding. The shorter the period of time, the greater the performance degradation because the instability will have had a longer time to deform the optics. The table also provides an estimate of the top level HRMA performance. These values were calculated by combining (via RSS) the on-orbit variation effects, currently 0.33, with the year by year 90% diameter values in Tables 1 & 2 and then summing these values with the on-orbit know bias, currently 0.62. This method somewhat overestimates the degradation because the 5 year mission effects are not broken out on a year by year basis but are lumped at the beginning of life. Also, the uniform effects of the material creep will offset the uniform effects of the nominal moisture loss.

3.3 Invar mount pads

Figures 23 through 25 show the invar instability, both in its raw data form and converted into PPM/yr. Two different heat-treatments were used. The standard EKC treatment and what is the so-called "MIT triple-treat" heat treatment . The three part heat treatment consists of a solution heat treatment (830C/ water quench) to lower the CTE of the invar, an intermediate heat treatment (385C/furnace cool) to relieve the quenching and machining stresses followed by a final low temperature (100C/slow oven cool) to redistribute the carbon and further relieve quenching and machining stresses. The EKC heat treatment was identical to that above but the intermediate 385C treatment was eliminated and another 100C cycle was added after the ends of the stability test samples were hand lapped. Results indicate that the EKC method provides a much more uniform stability than does the MIT method. Some data suggests that heat

treatments above 205C may be responsible for carbon being driven out of solution which promotes grain growth which can adversely affect the invars' stability. The invar material used was a hot-rolled CYCLOPS UNISPAN LR35 with a carbon content of 0.057%. The CTE from the factory was +0.13PPM/C.

The form of the data are fit well by a single exponential (unlike data obtained by Steele (ref 18) which indicates both short and long term exponentials). It may have been that our testing did not start soon enough after final heat treatment to pick up the initial short term response.

The instability of the invar pads is manifested by dimples in the optics which extend radially outward from the pads approximately 0.1m and which have peak to valley distortions of about 0.03 microns per PPM invar strain. The magnitude of this deformation assumes that the epoxy does not ameliorate the invar strain. The performance degradation per PPM invar instabilty is about 0.04 arc sec.

3.4 Zerodur optics

Both the raw data and the converted data for Zerodur are shown in figures 26 & 27. The d3 sample, figure 26 is slightly noisier than sample d7 and its instability is 3-4 times worse (0.03 vs 0.008 PPM/yr). We have no explanation for this difference except the possibility that the Tor-Seal bonding may play a part in the difference. That being the case, the limit on the accuracy of the tests using the "open book" configuration may be limited to the order 0.03 PPM/yr.

3.5 6061 aluminum

EKC originally planned to fabricate the OSC from 6061 T6 aluminum. However, with the experience gained with the 7050 T7451, including its greater strength, a material change was made. The data for the 6061 is presented here as figures 28 through 30 is for reference only. All three samples exhibited instabilities of < 1.0PPM/yr near the end of the test period.

3.6 Reference materials SiO_2, invar LR-35, copper

Figures 31 - 33 show both the raw data and the converted data (into PPM/yr) for the materials used as references. During the entire test period, the SiO_2 frequency remained virtually constant. The LR-35 invar had been measured many times over the past 20 years. Its' current instability is about 0.10 PPM/yr. Previous measurements of this sample (op. cit.) indicated an initial growth rate of about 2 PPM/yr in 1976 and < 0.01 PPM/yr in 1991. Daily temperature fluctuations of the copper reference are shown in figure 33. For most of the testing, the average daily temperature remained within a band of +/- 0.01C and over the test period decreased about 0.002C.

4 CONCLUSIONS

Precise space-based optical systems require the use of materials whose dimensional instability is minimal or whose effect can be mitigated by the design itself. For the most part, design of the AXAF-I HRMA is quite robust. In general, large uniform instabilities do affect the telescopes' performance. The one area of concern are the invar pads which are currently under test in a flight-like configuration. We believe that the top level AXAF-I requirements will be met using the stability data already in hand coupled with the data on the invar currently being tested.

The challenges that were required to produce and analyze these data were not insignificant. The environment that the samples were fabricated in, stored in and tested in all affected the results. The time from final fabrication to test time was found to be a significant contributor in lessening the performance degradation effects. The longer the duration between final part fabrication and the time when the part is to be installed into its system goes a long way to reducing the performance impact. Long range planning is essential such that materials can be tested well in advance of their need dates.

5 ACKNOWLEDGEMENTS

I wish to thank NASA/MSFC for funding this study. Special thanks go to J.P. Zheng who performed most of the CAP FE analysis and data analysis. Thanks also go to E. Whitbeck & Y. Zhou for many of the figures that were used. Thanks also go to W. Reitz of EKC for providing data on the tested materials. Finally, I wish to thank all of the other personnel at SAO, MSFC, TRW, EKC, and Hercules who contributed in the many discussions and reviews that were held on this subject.

6 REFERENCES

[1] Sable. W. W., "A probabilistic model of the thermal dimensional stability of composite structural components, *SPIE*, 1690, pp 323-328, 1992

[2] Marschall, C, Maringer, R, "Dimensional Instability An Introduction", pg 217, Pergamon Press, 1977

[3] D.E. Schwab, S.R. Jacobs, S.C. Johnston, "Osothermal Dimensional Instability of Invar", *proceedings of the 29th Nationals SAMPE Symposium*, 169 (1984)

[4] Private communication between A. Tao of TRW and SAO

[5] Dolgin B., "Assessment of Dimensional Stability Technology for Future NASA Missions", *JPL report JPL D-9140*, 1992

[6] Berthold, J.W. III, Jacobs, S.F., Norton, M.A., "Dimensional Stability of Fused Silica, Invar, and Several Ultra-low

[7] Kodak-SE11w, Vol 1 of 5, Tech Notes "AXAF-93-005 Stone, Monte-Carlo Program and Methodology" and "AXAF-93-0012-Thrasher, Sleeve CTE Variation With Flexure Interface On Eight Cell Models", 1993

[8] Cohen, L.M. & Zhang, J.P., "Final Report, The Effects of Temporal Instability of the Aluminum Central Aperture Plate on the AXAF-I HRMA Optical Performance" , *SAO-AXAF-DR-94-110*, 1994

[9] Cohen, L.M., Freeman, M.D., Podgorski, W.A., Temporal Instability of Graphite-Cyanate Ester Composites and Its Effect on the High Resolution Mirror Assembly of the NASA Advanced X-ray Astrophysics Facility, *1995 SEM Spring Conference*, 1995

[10] Private communication between M. Nowers of Hercules and SAO.

$$\Delta f(t) = -474 \cdot CME \cdot M_0 \cdot \left[e^{-\left(3.7 \cdot \left(D \cdot t / h^2\right)\right)^{0.577}} - 1 \right]$$

where

$\Delta f(t)$	=	*Sample frequency(MHz) change vs. Time*
t	=	*Time in hours since start of test #1(5/21/93)*
-474	=	*Conversion from ppm to MHz*
CME	=	*125ppm/% moisture*
M_0	=	*Initial moisture content(%)*
D	=	*Diffusivity - 2.04x10^{-6} in^2/hr@70 deg F*
h	=	*Thickness(0.25")*

[11] Private communication between M. Nowers of Hercules and SAO

[12] Private communication between Dr. M. Puckett, Dow-Corning Inc. and L. Cohen of SAO

[13] Private communication between Prof. S. Tsai, Stanford University and L. Cohen of SAO

[14] Private communication between Prof. D. Dillard of VPI and L. Cohen of SAO

[15] Private communication between Prof. M. Tuttle of Uinv. of Washington and L. Cohen of SAO

[16] Private communication between D. Powell of ICI Fiberite and L. Cohen of SAO

[17] Private communication between Prof. M. Tuttle of Univ. of Washington and L. Cohen of SAO

[18] Steele, J.M., et al, " Temperature and Age Effects on the Temporal Stability of Invar", *SPIE* Proc. **1752**, (1992)

Table 1
Predicted CAP Instability Effetcs
(Arc Seconds, 90% Diameter, 2-Sigma)

SHELL	@ LAUNCH	@End-of-Life
P1/H1	0.009	0.010
P3/H3	0.023	0.029
P4/H4	0.042	0.057
P6/H6	0.065	0.075
HRMA*	0.026	0.032

Table 2
Predicted Mirror Support Sleeve Instability Effetcs
(Arc Seconds, 90% Diameter, 2-Sigma)

SHELL	@ LAUNCH	@End-of-Life
P1/H1	0.069	0.092
P3/H3	0.108	0.142
P4/H4	0.140	0.180
P6/H6	0.118	0.149
HRMA*	0.099	0.129

HRMA @ Top Level	0.966	0.976

* HRMA values are area weighted @ 0.277KeV

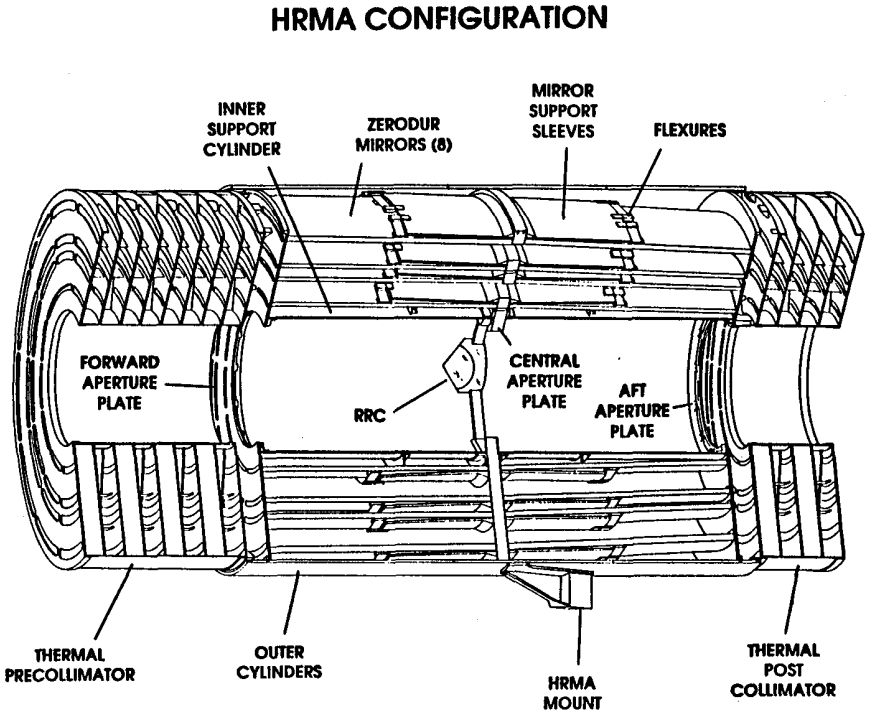

Fig. 1- HRMA Configuration

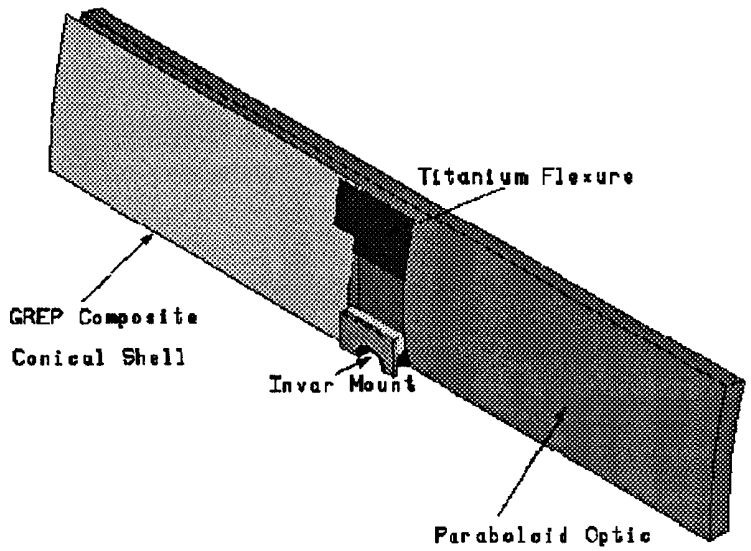

Fig. 2- Section of Mirror Cell

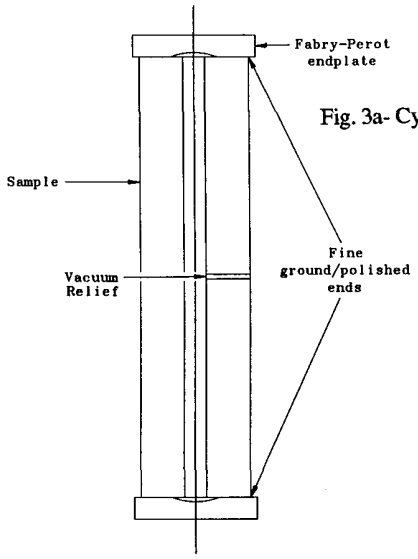

Fig. 3a- Cylindrical Geometry

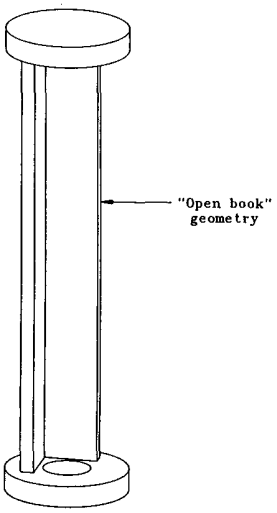

Fig. 3b- "Open Book" Geometry

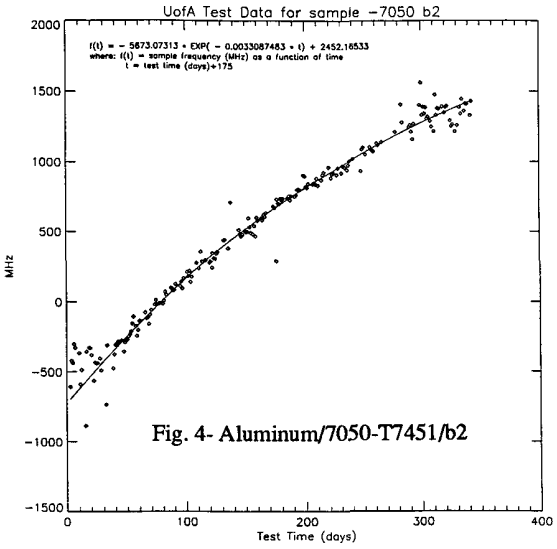

Fig. 4- Aluminum/7050-T7451/b2

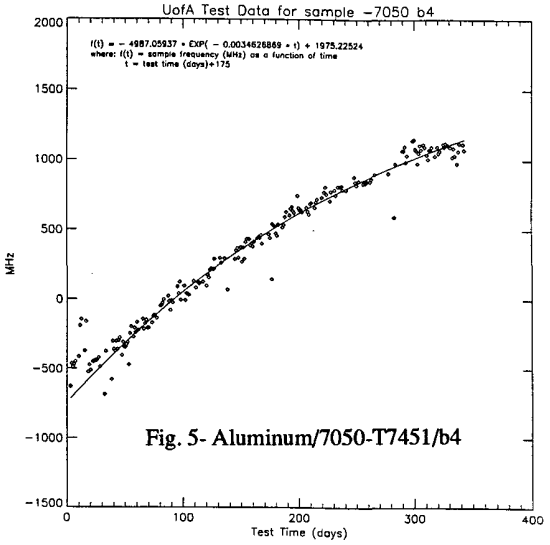

Fig. 5- Aluminum/7050-T7451/b4

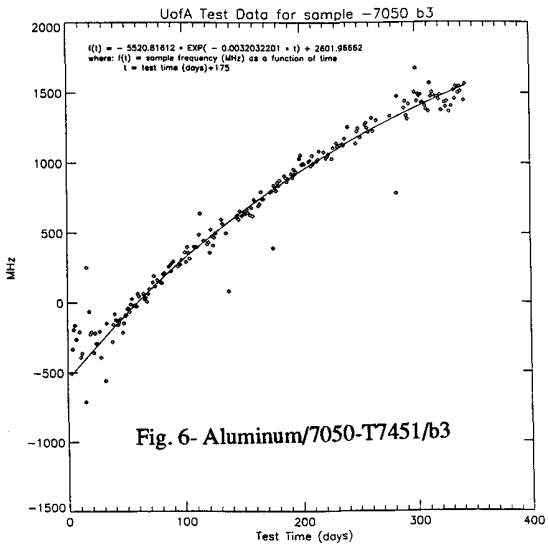

Fig. 6- Aluminum/7050-T7451/b3

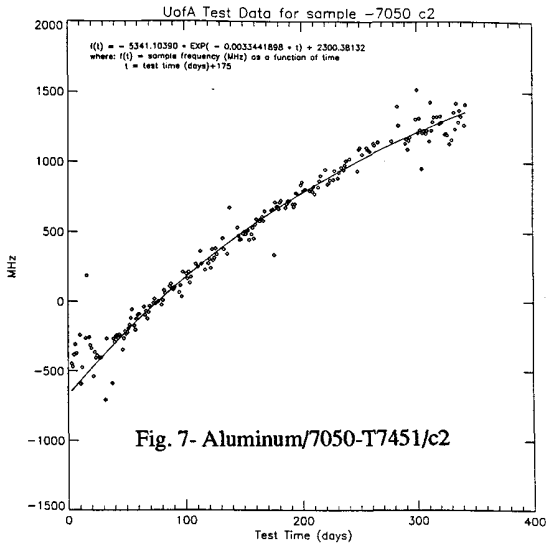

Fig. 7- Aluminum/7050-T7451/c2

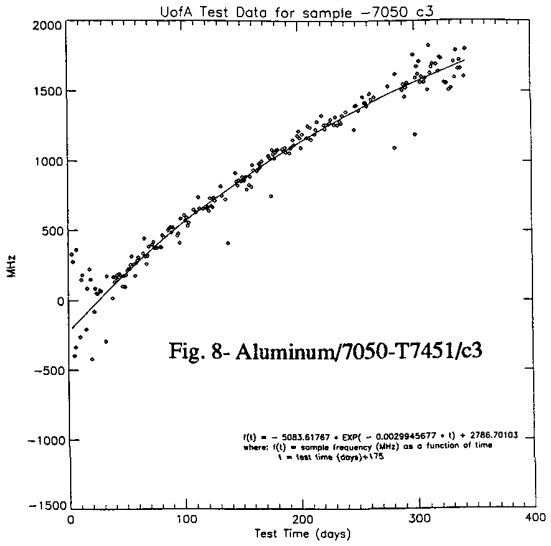

Fig. 8- Aluminum/7050-T7451/c3

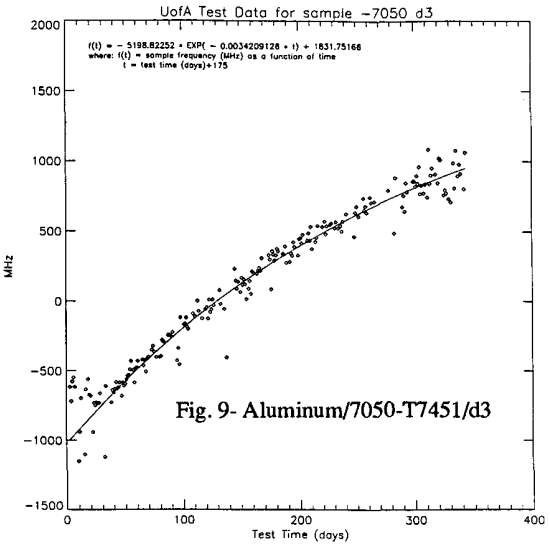

Fig. 9- Aluminum/7050-T7451/d3

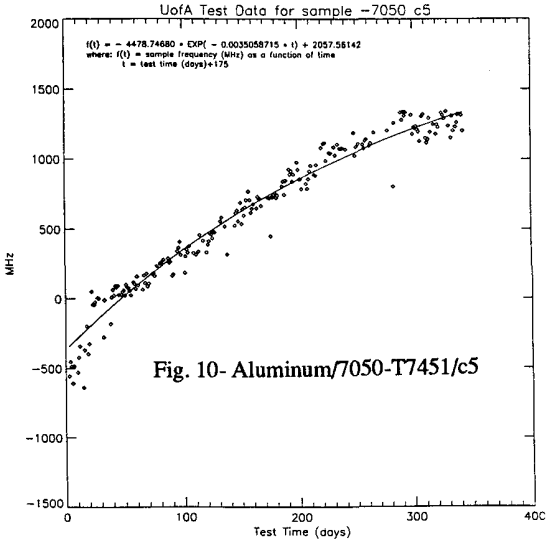

Fig. 10- Aluminum/7050-T7451/c5

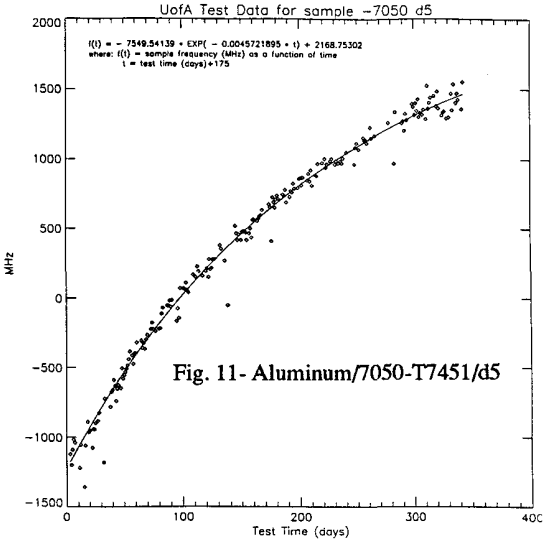

Fig. 11- Aluminum/7050-T7451/d5

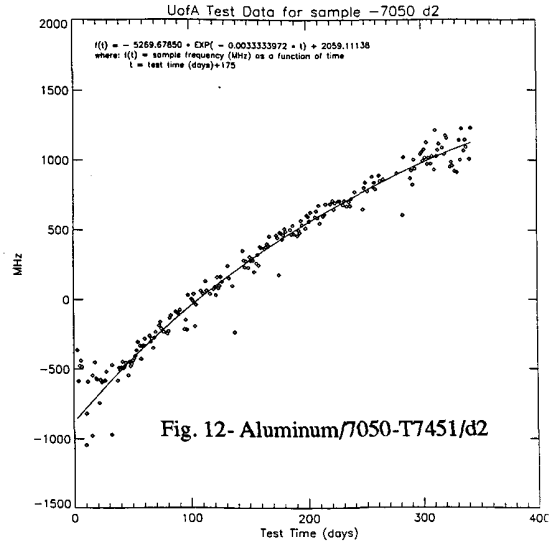

Fig. 12- Aluminum/7050-T7451/d2

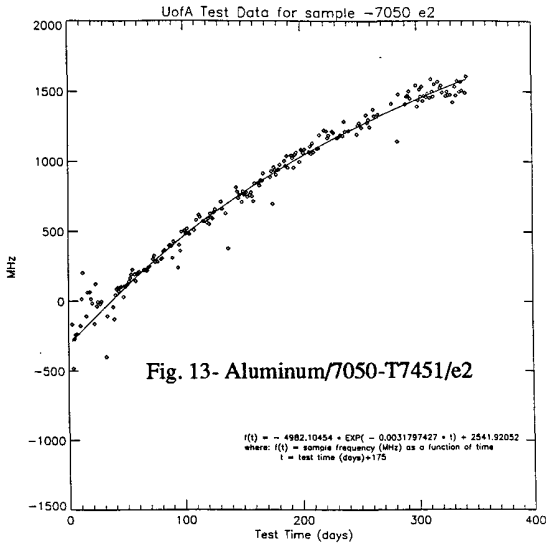

Fig. 13- Aluminum/7050-T7451/e2

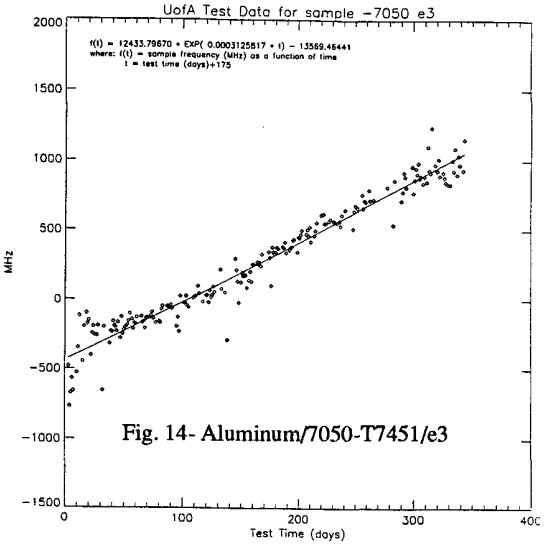

Fig. 14- Aluminum/7050-T7451/e3

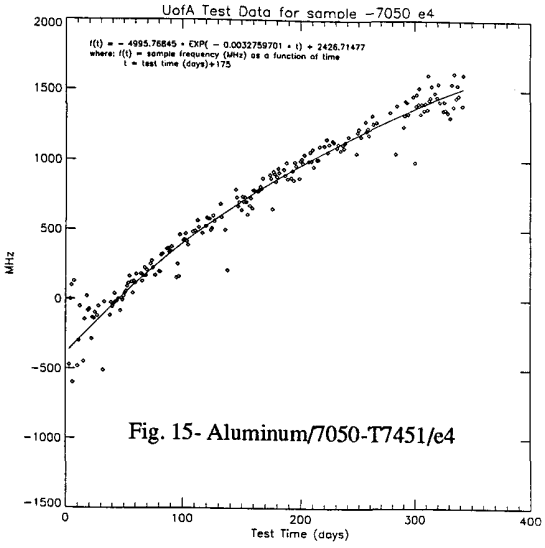

Fig. 15- Aluminum/7050-T7451/e4

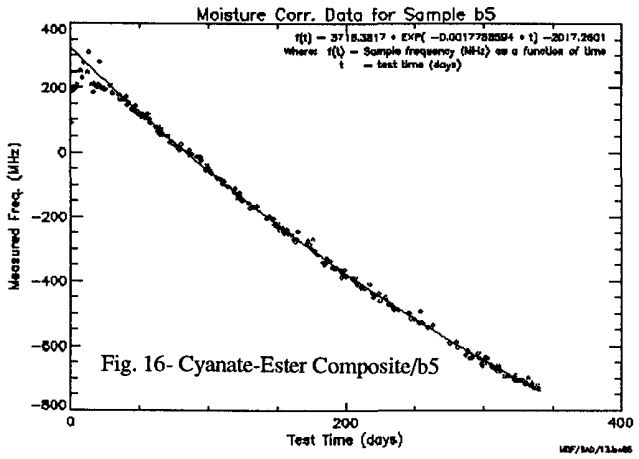

Fig. 16- Cyanate-Ester Composite/b5

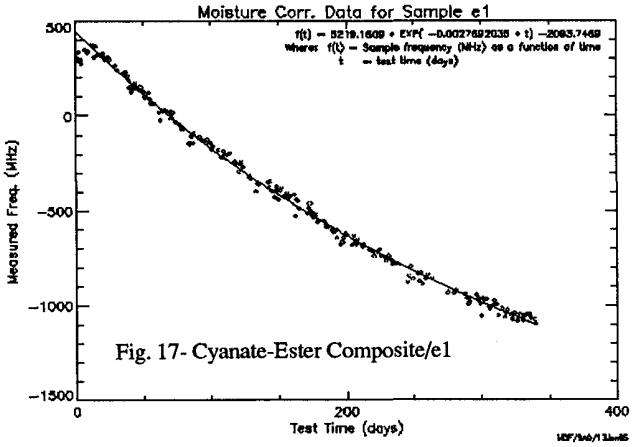

Fig. 17- Cyanate-Ester Composite/e1

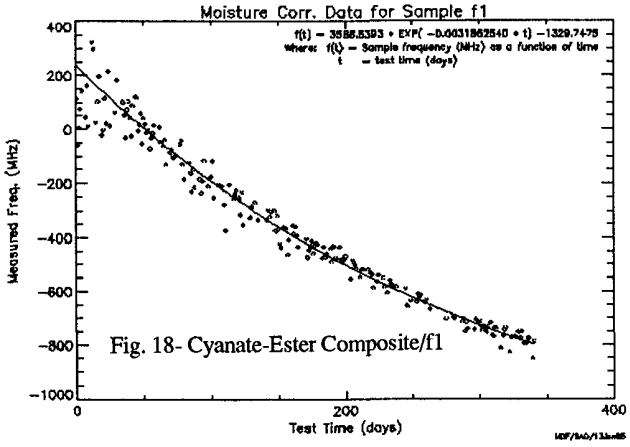

Fig. 18- Cyanate-Ester Composite/f1

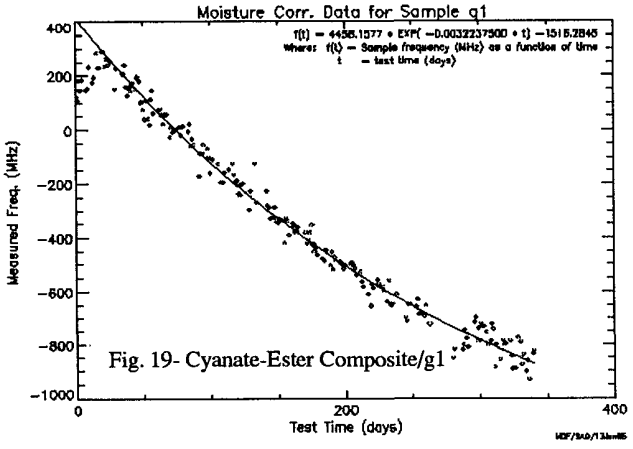

Fig. 19- Cyanate-Ester Composite/g1

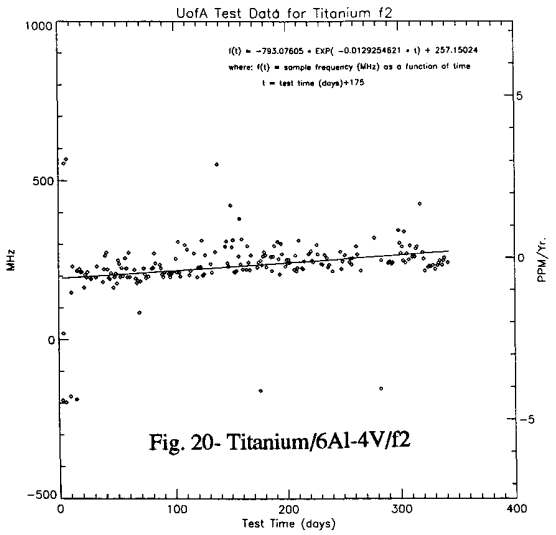

Fig. 20- Titanium/6Al-4V/f2

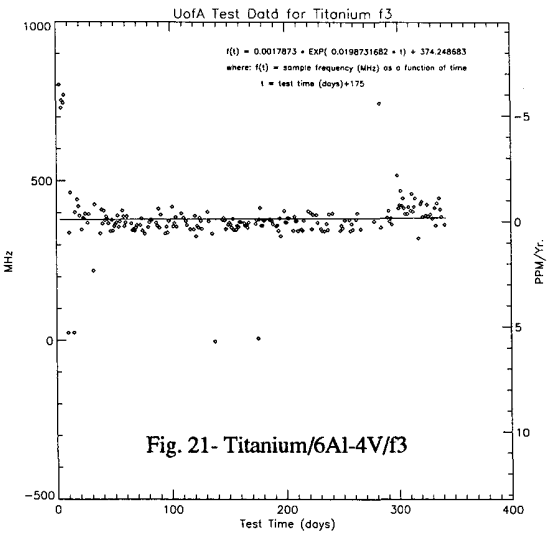

Fig. 21- Titanium/6Al-4V/f3

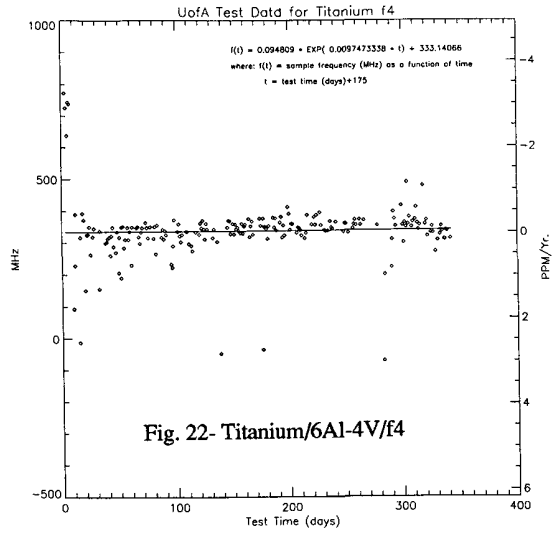

Fig. 22- Titanium/6Al-4V/f4

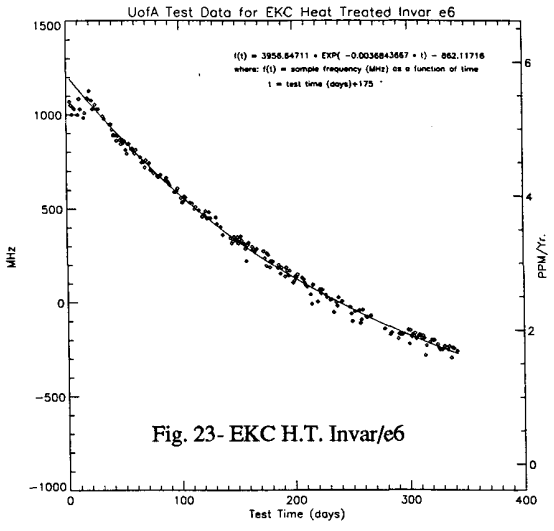

Fig. 23- EKC H.T. Invar/e6

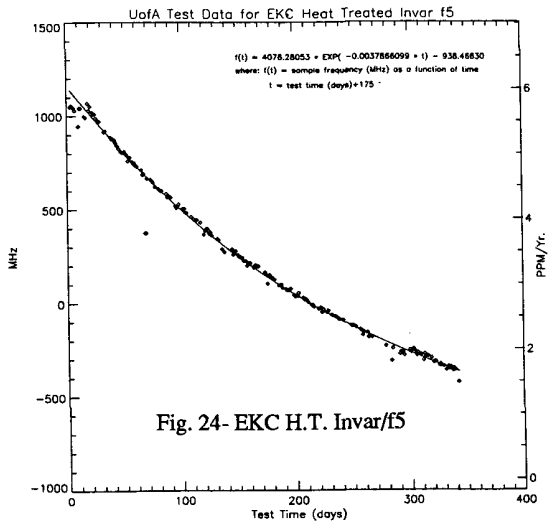

Fig. 24- EKC H.T. Invar/f5

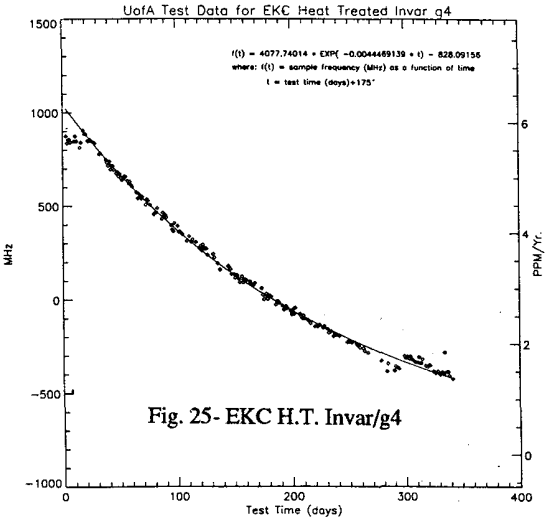

Fig. 25- EKC H.T. Invar/g4

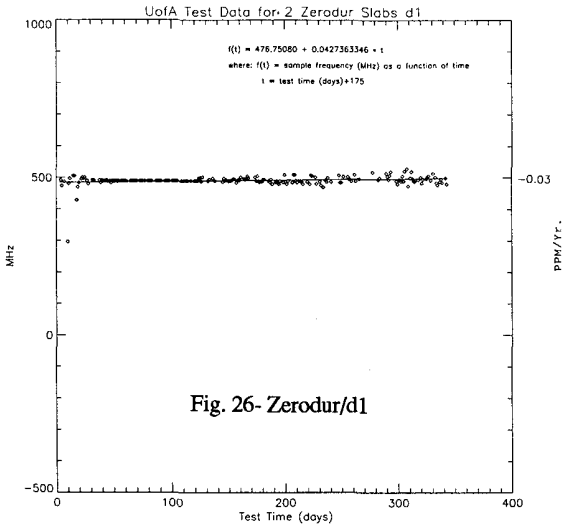

Fig. 26- Zerodur/d1

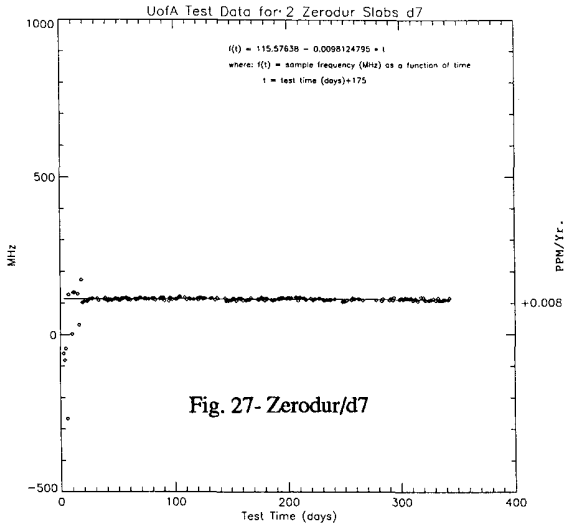

Fig. 27- Zerodur/d7

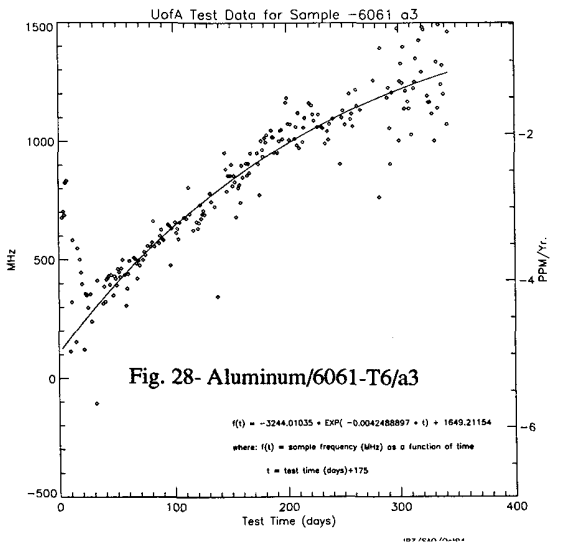

Fig. 28- Aluminum/6061-T6/a3

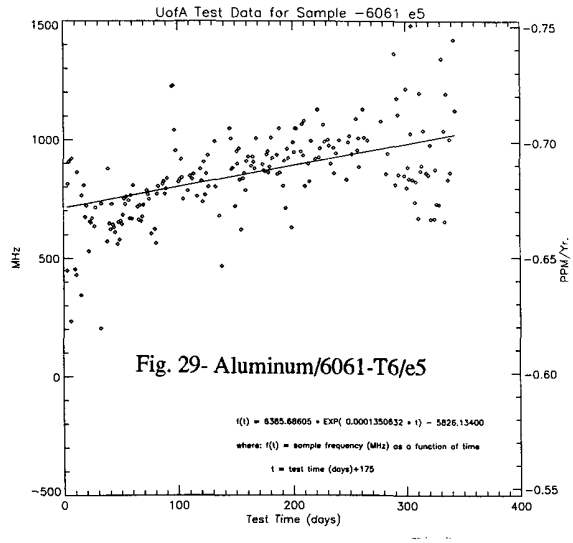

Fig. 29- Aluminum/6061-T6/e5

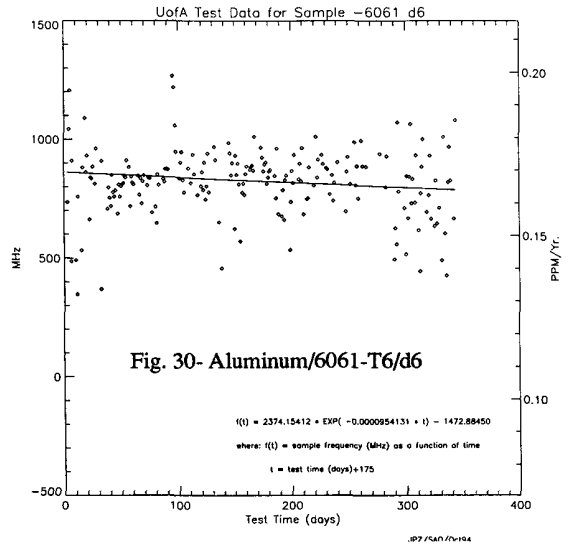

Fig. 30- Aluminum/6061-T6/d6

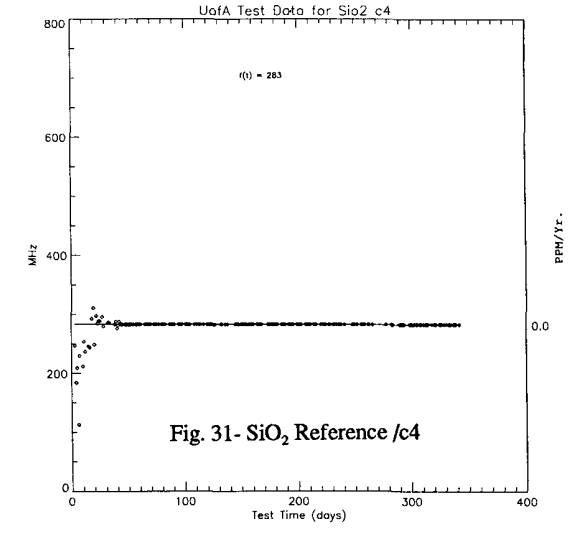

Fig. 31- SiO_2 Reference /c4

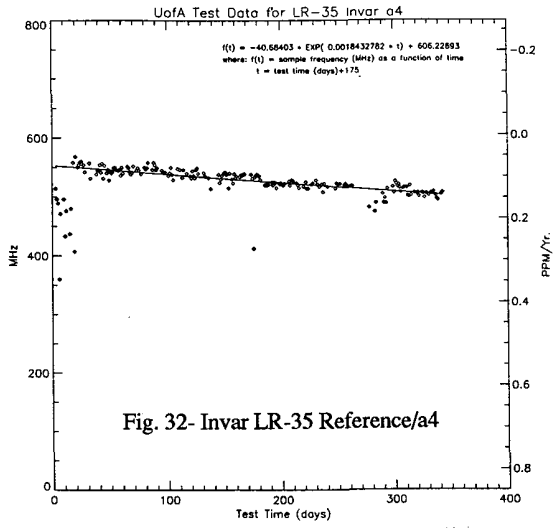

Fig. 32- Invar LR-35 Reference/a4

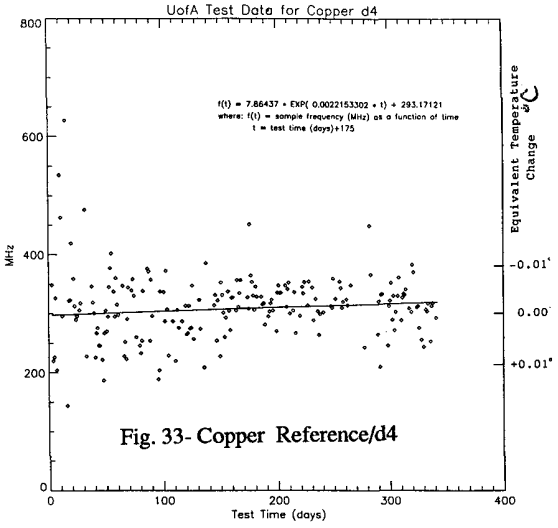

Fig. 33- Copper Reference/d4

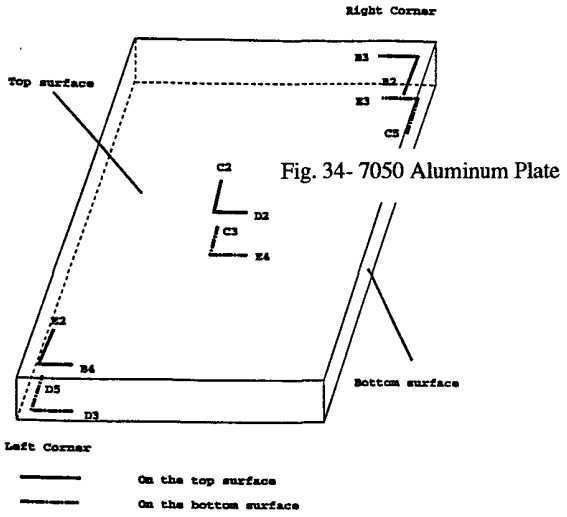

Fig. 34- 7050 Aluminum Plate

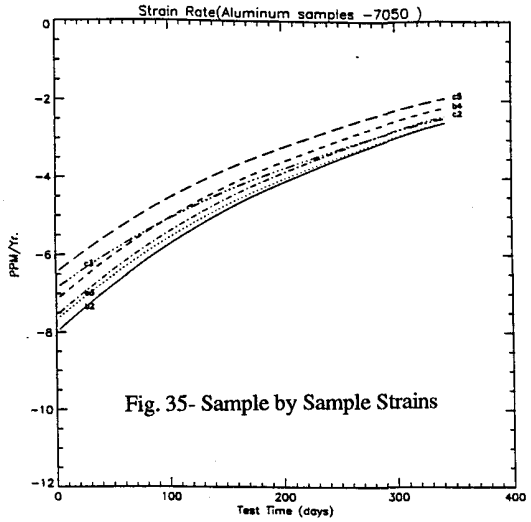

Fig. 35- Sample by Sample Strains

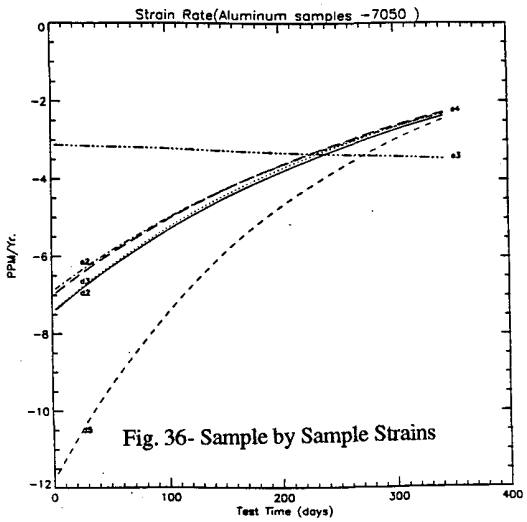

Fig. 36- Sample by Sample Strains

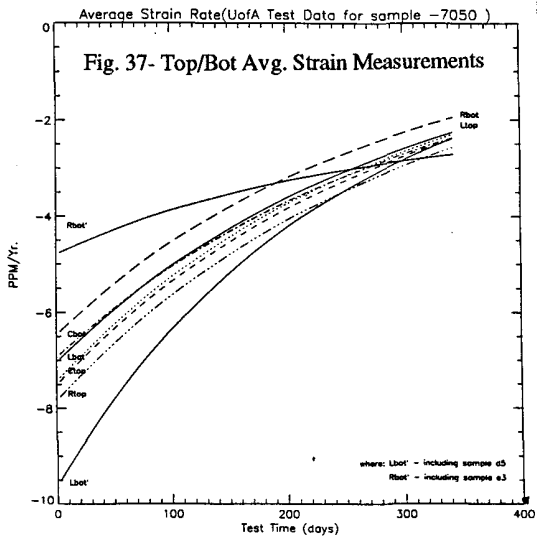

Fig. 37- Top/Bot Avg. Strain Measurements

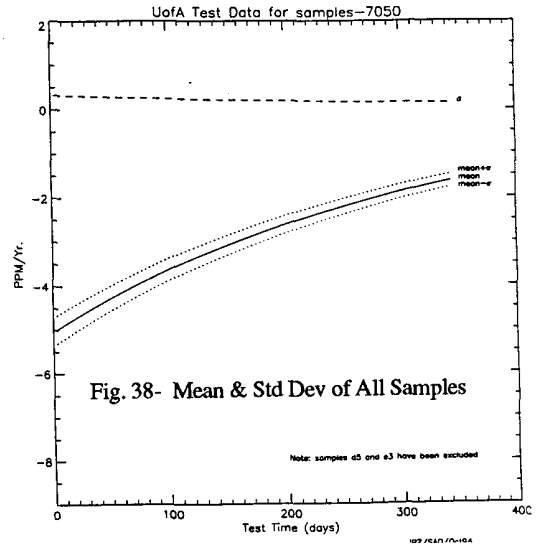

Fig. 38- Mean & Std Dev of All Samples

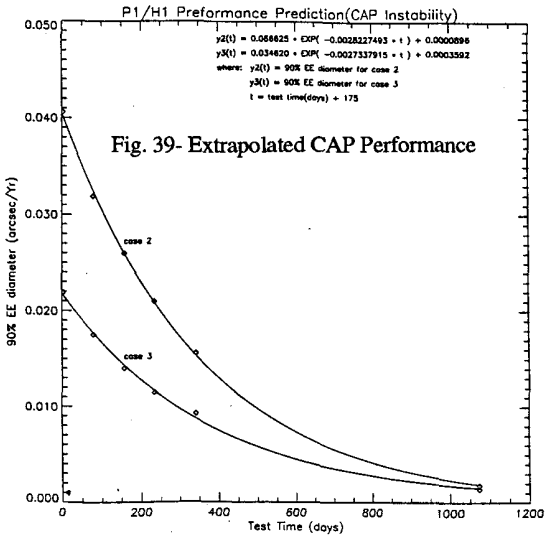

Fig. 39- Extrapolated CAP Performance

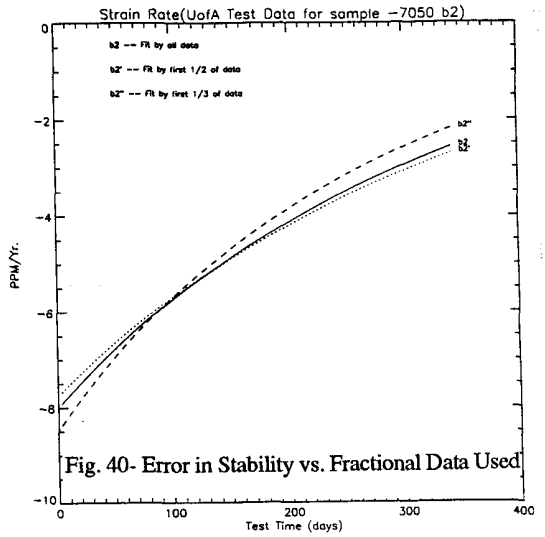

Fig. 40- Error in Stability vs. Fractional Data Used

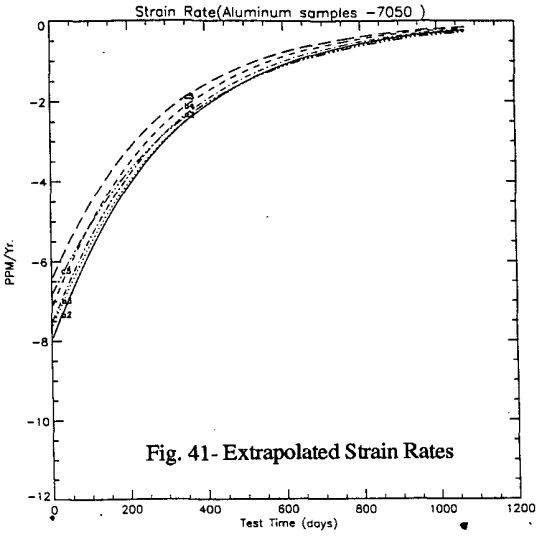

Fig. 41- Extrapolated Strain Rates

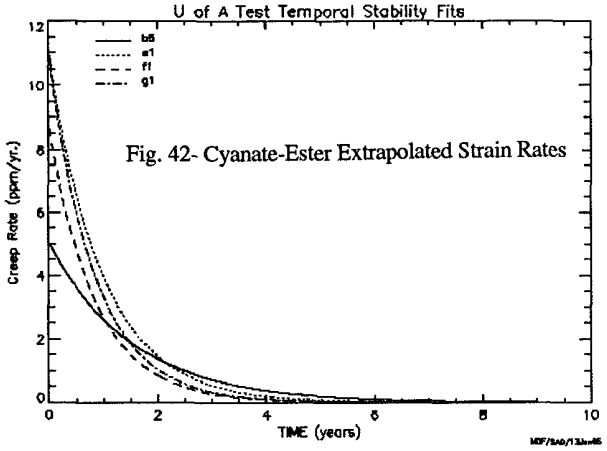

Fig. 42- Cyanate-Ester Extrapolated Strain Rates

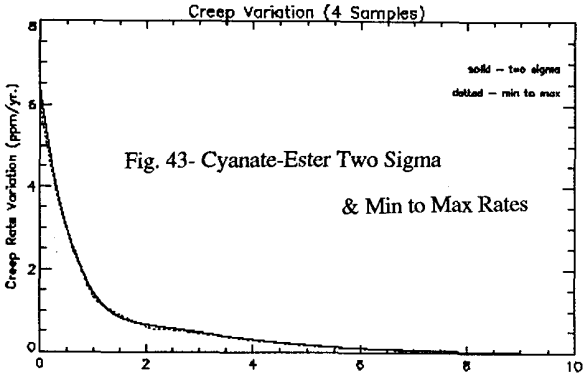

Fig. 43- Cyanate-Ester Two Sigma & Min to Max Rates

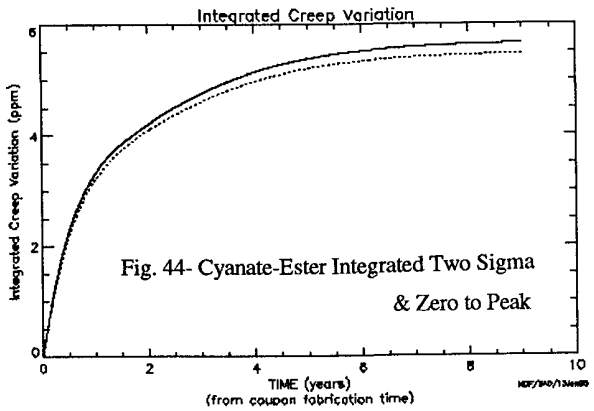

Fig. 44- Cyanate-Ester Integrated Two Sigma & Zero to Peak

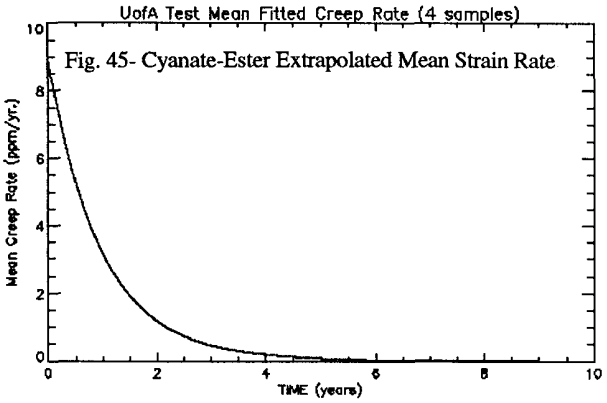

Fig. 45- Cyanate-Ester Extrapolated Mean Strain Rate

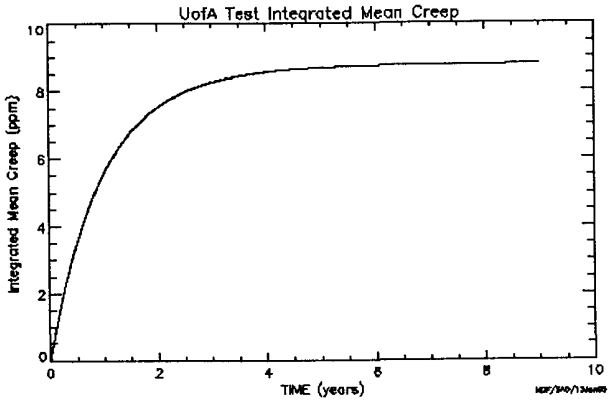

Fig. 46- Cyanate-Ester Integrated Mean Strain

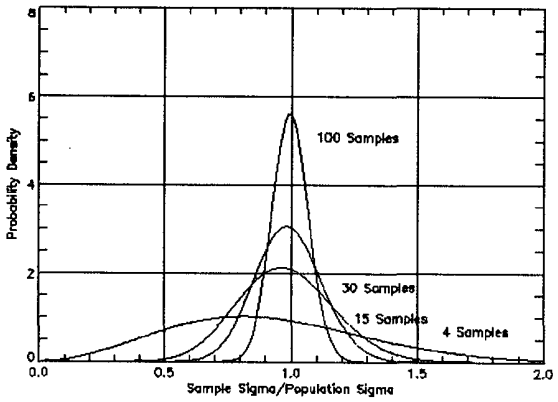

Fig. 47- Sample Size Effects